JOURNAL OF CATALYSIS 44, 373–384 (1976)

Thermal Desorption Studies of CO and H_2 from the Cu–Ni Alloy

K. Y. Yu, D. T. Ling, and W. E. Spicer

Electrical Engineering Department, Stanford University, Stanford, California 94305

Received April 5, 1976

The desorption order and activation energies of CO and H_2 from a (110) oriented Cu–Ni single crystal have been studied by thermal desorption spectroscopy. The surface composition of the alloy can be varied by annealing (after sputtering treatment which reduces the surface Cu concentration) in a temperature range where the surface composition is controlled by bulk diffusion. The surface composition is determined by the relative line intensities of the Auger $M_1M_{4,5}M_{4,5}$ Cu and Ni transitions at $\simeq$100 eV electron energy, and therefore represents an average concentration measurement within the electron escape length (approximately the first couple of atomic layers). The CO desorption spectra are mainly interpreted in terms of the ensemble effect, which relates the heat of chemisorption to the number and the species of the surface atoms in contact with the CO molecule. The CO desorption kinetics is first order. Four desorption states are resolved, two of which are readily identified as desorption from a pure Cu or pure Ni ensemble (i.e., pure Cu or pure Ni binding site). The pure Ni binding state activation energy decreases linearly with increasing surface Cu concentration, indicating that a ligand (long range) effect is also present in the bonding. The H_2 desorption kinetics is second order. Two binding states are resolved, and both of them are shown to have a pure Ni origin. The activation energy of the high temperature bonding state remains constant with changing surface composition.

A. INTRODUCTION

The study of the adsorption and catalytic property of alloys has been an extremely active area (*1–6*). Several important concepts have evolved through studies of alloys formed by group VIII and group IB transition metals. One of such concepts is the ensemble effect (*7–11*), which views that the strength of the chemisorption bond is determined by surface atoms immediately adjacent to the adsorbed molecule (i.e., by the atoms constituting the binding site). Thus, changing the number or the species of the surface atoms in the binding site affects the bond strength directly. The ensemble effect is an extremely important concept since it forms the basis for the interpretation of a host of adsorption phenomena (*7–11*),[1] involving not only the alloys but other transition metals as well. In the past years, Sachtler and co-workers and other researchers (*12–18*) have studied the adsorption and catalytic properties of the Cu–Ni alloy extensively. In most of the work, evaporated Cu–Ni films were used as samples, and experimental techniques based on work function measurements, H_2 titration, infrared spectroscopy, and measurements of catalytic activity of test reactions were employed. The surface composition of the alloy films could be measured only indirectly. Sachtler has

[1] For example, the determination of the number of active sites on a catalyst by H_2 or CO titration would only make sense if the atoms forming the bonding site retain their atomic characters.

suggested that the ensemble effect may adequately describe the alloy's chemisorption and catalytic behavior, although he also recognized the possibility of non-nearest neighbor (long range) effects (*19*).

Although the influence of atoms away from the adsorption site has been deemphasized, it is well known from other studies (*20–22*) that non-nearest neighbor effect (long range effect) does affect the overall electronic structure of the alloy. For example, the electronic structure of the Cu–Ni alloy is relatively well understood in terms of theoretical models such as the Coherent Potential Approximation (CPA) (*21*) or the Average T-matrix Approximation (ATA) (*22*). Certain features of the alloy density of states, such as the width of the Ni virtual level on Cu-rich alloy, has been related to long range d-electron interaction (*21*). It is expected that similar long range interaction can affect the chemisorption properties of the alloy. Following the terminology used in transition metal chemistry, we will denote any non-nearest neighbor influence on a chemisorption bond as a ligand effect.

In order to examine more closely the interplay of the ensemble effect and ligand effect in the bonding of simple molecules on transition metals and to assess their relative importance, we have performed thermal desorption experiments of CO and H_2 on well-characterized Cu–Ni alloy surfaces, under conditions which meet the standards of modern surface science. All experiments were performed in ultrahigh vacuum (10^{-10} Torr). The surface composition of the alloy sample was measured directly by Auger Electron Spectroscopy (AES), and the surface crystallinity monitored by LEED. The ability to measure the alloy surface composition directly and to keep a clean working surface in good vacuum represented a significant improvement over previous alloy film work. The desorption order and activation energies of CO and H_2 were studied as a function of alloy surface composition and the results are discussed in terms of the ensemble and ligand effect.

B. EXPERIMENT

The single Cu–Ni alloy sample studied is a (110) oriented single crystal grown by the Bridgeman technique. Its atomic composition is 10% Cu–90% Ni. After alignment to a few degrees of the desired orientation by the Laue back reflection method, thin slices ($\simeq$30 mils) were cut, polished and etched to a mirror finish, as described previously (*23–25*). A slice of the sample was then mounted on a sample flange having 270° rotational freedom. A liquid nitrogen reservoir and copper cold strap combination was capable of cooling the sample down to −110°C. The chamber was equipped with a Varian 4-grid LEED-Auger energy analyzer, a PHI glancing incidence Auger electron gun, a Varian argon ion sputter gun, and a UTI-100 C mass spectrometer. To obtain an atomically clean surface, the sample was successively sputtered by a beam of argon ions and then annealed. The anneal temperature had to be high enough to enable the bulk sulfur impurities to diffuse to the surface so that they could be sputtered away during the next sputtering cycle. Since it was found that annealing at 650°C for a few minutes was sufficient to give an alloy surface composition close to equilibrium (*24*) (see Section C), the same annealing temperature was used during the sputter-anneal cycles. This was purely a matter of convenience because an anneal temperature as low as 500°C was sufficient to bring out the sulfur atoms. The sample was heated either radiatively by a tungsten filament located behind the sample, or by electron bombardment, during which the tungsten filament acted as the cathode and the sample as the anode, with 2.5 kV applied between them.

C. DIFFUSION CONTROLLED SURFACE COMPOSITION

Before the method used to prepare alloy surfaces of different compositions can be described, we must clarify the operational meaning of surface composition. The alloy surface composition was determined by taking the ratio of the intensities of the Auger $M_1M_{4,5}M_{4,5}$ Cu and Ni transitions at approximately 100 eV. (Using 1 V modulation voltage these peaks can be separated without difficulty.) Since the measurements were made consistently from surface to surface, the relative accuracy should be better than $\pm 10\%$. The electron escape length at 100 eV electron energy was estimated to be one or two atomic layers (*24*). Hence, the Auger "surface composition" represents an average concentration measurement within the electron escape length (i.e., one or two atomic layers).

Based on fairly general thermodynamic arguments, several theories (*26–28*) have predicted that the alloy component with the lowest bond energy would segregate to the surface of the binary alloy at thermal equilibrium. However, because of the difference in surface and bulk diffusion coefficients (see Fig. 1), one may regrow (after sputtering) a crystalline surface after annealing at temperatures much lower than those necessary for producing an equilibrium surface composition. Helms (*23*) and Helms and Yu (*24*) have reported AES measurements on the surface composition (as defined above) of the Cu–Ni alloy. After annealing the alloy samples at 650°C for 10–15 min and then quenching them to room temperature, substantial amount of Cu enrichment on the surface was found. Annealing the samples at higher temperatures did not produce any more Cu segregation. Therefore, the alloy surface annealed to 650°C was assumed to have reached thermal equilibrium. The relatively high annealing temperature of 650°C was required to observe segregation because the bulk alloy diffusion process was extremely sluggish (*29*), which impeded the attainment of true surface-bulk equilibrium at low temperature. Taking advantage of the slow bulk diffusion process, we have prepared an alloy surface of different compositions from the same sample by a technique of interrupted annealing. Figure 1 shows the measured bulk diffusion constant for Cu–Ni alloys and pure Cu as well as the surface diffusion constant for pure Cu (*30*), in the temperature range of 300°C to 1000°C. The steepness of the bulk diffusion curve indicates that the bulk diffusion process has a high activation energy. Note that $d = (Dt)^{\frac{1}{2}}$, where d is the distance traveled by diffusion in time t, with a diffusion constant D. From Fig. 1, $D \approx 10^{-16}$ cm²/sec at 450°C. Therefore, $d \approx 1$ Å for $t = 1$ sec, which means that the bulk alloy atoms are, for all practical purposes, immobile until a temperature of above 450°C is reached. To prepare an alloy surface of a desired composition, the sample

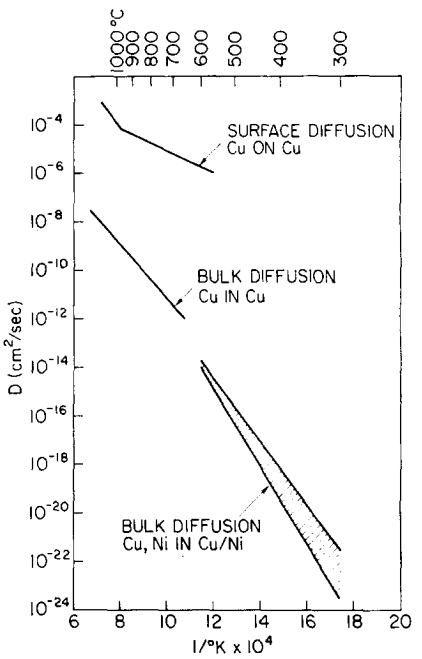

FIG. 1. Surface and bulk diffusion constant of pure Cu and Cu–Ni alloy versus temperature.

TABLE 1

Annealing Schedule Versus Surface Composition

Temperature (°C)	Surface composition
No annealing (after sputtering)	100% Ni
440 for 2 min	82% Ni–18% Cu
475 for 1 min	75% Ni–25% Cu
510 for 2 min	65% Ni–35% Cu
555 for 2 min	60% Ni–40% Cu
600 for 1 min	52% Ni–48% Cu
625–650 for 2 min	35% Ni–65% Cu

was first sputtered by a beam of 300 eV argon ions for 5 min. Since Cu is sputtered preferentially from the alloy surface (*31*), the sputtered alloy surface has a surface composition of approximately 100% Ni (*24*). Then depending on the desired surface composition, the sample was carefully annealed in the temperature range of 440 to 650°C for 1 to 2 min, and quickly quenched to room temperature. We have succeeded in producing an alloy surface whose composition ranges from 82% Ni to 35% Ni. The annealing schedule and the resulting surface compositions as determined from Auger are tabulated in Table 1.

Although the alloy surface is not in equilibrium with the bulk, the surface composition is stable at room temperature, as expected from the small bulk diffusion constant. Any of the above surface compositions is quite reproducible if the same annealing schedule is followed. Furthermore, the adsorption and thermal desorption of CO of H_2 do not change the surface composition, which has been confirmed by Auger measurements before and after desorption measurements. This is reasonable since all desorption experiments were carried out below 200°C, where one would not expect any significant mobility of the alloy atoms.

Preliminary LEED studies gave evidence that even the lowest annealing temperature used in this work was sufficient to cure the surface damages caused by sputtering, and to restore the surface crystallinity. On the sputtered surface, only a diffuse pattern was observed. A short anneal cycle of 2 min at 440°C was sufficient to bring out a 1 × 1 LEED pattern. The 1 × 1 pattern sharpened somewhat after annealing to 500°C and remained unchanged at higher annealing temperatures. The reason is again found in Fig. 1. The surface diffusion constant is approximately five orders of magnitude higher than the bulk diffusion constant (*30*). Thus, even though the annealing temperature is not high enough to fully restore surface-bulk equilibrium, it is more than enough to repair surface damages.

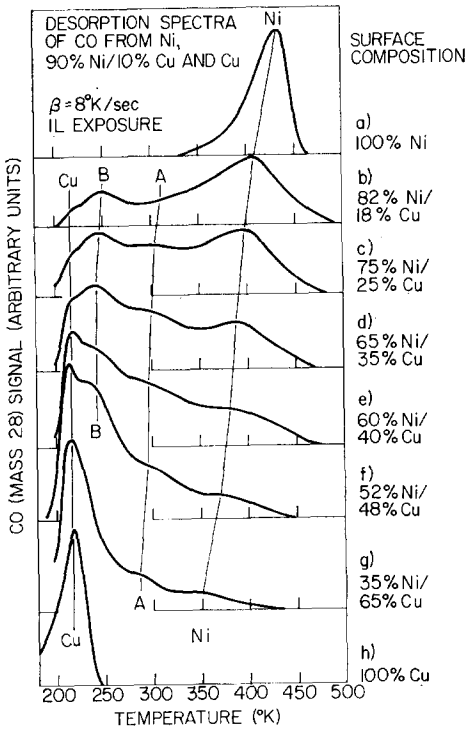

FIG. 2. Thermal desorption spectra of CO from Ni (110), 10% Cu–90% Ni (110) bulk alloy with different surface compositions, and Cu (110). CO was adsorbed at −100°C (173°K). The datum on Ni (110) is taken from Ref. *32*. β = linear heating rate in °K/sec. The highest desorption temperature was sufficiently low so that the surface composition of the alloy was unchanged by the adsorption–desorption cycle.

D. CO DESORPTION FROM Cu, Ni, AND Cu–Ni ALLOY SURFACES

1. Desorption Spectra

In Fig. 2, the CO desorption spectra of Ni (110), alloy surface of different compositions, and Cu (110) are presented. These curves were taken at 1 L (10^{-6} Torr-sec) exposure, which was close to the saturation exposure of 3 L. The surface compositions measured by AES are indicated on the right-hand side of the figure. To understand the desorption characteristics of the alloy surfaces, it is necessary to know the desorption behavior of the endpoints of the alloys, i.e., pure Cu and Ni. The data on Ni (110) (Fig. 2a) was taken from the work of Falconer and Madix (*32*). They have shown that up to an exposure of 2 L, a single first-order desorption peak was resolved. Since no desorption data was available on Cu, we have performed CO desorption experiments on Cu (110), from which the curve for 1 L exposure was shown in Fig. 2h. Unfortunately, our cooling temperature of −110°C was insufficient to resolve the CO desorption peak completely. At any rate, only one desorption peak was seen up to saturation coverage (3–10 L), and the peak temperature stayed constant as a function of coverage. This, together with photoemission evidence that CO adsorbs as a molecule, strongly suggests that CO desorption from Cu (110) is first order. Isosteric heat measurements have established that the heat of adsorption of CO on Cu (15 kcal/mol) (*33*) is about half as much as that on Ni (30 kcal/mol) (*34*, *35*). Note that the CO desorption peak temperature on Cu ($T \leq 220$°K) is also very close to half of that on Ni ($T = 440$°K), which is in agreement with the isosteric heat measurements. The alloy surface desorption spectra are considerably more complicated, and the next two sections will be devoted to their analyses.

2. Ensemble Effect on the Bonding of CO on the Alloy

On the alloy surfaces, four desorption peaks are resolved (Fig. 2b–g). The lowest temperature desorption peak at 220°K is associated with desorption from a pure Cu ensemble (or site) because the peak position coincides with the pure Cu peak (Fig. 2h). The highest temperature peak is associated with desorption from a pure Ni ensemble (or site), since, as the surface Ni concentration increases, its peak desorption temperature approaches that of pure Ni (Fig. 2a). In fact, the CO desorption peak temperature on the sputtered alloy surface (100% Ni surface composition) is approximately the same as on pure Ni (*25*). The Ni peak shifts by 80°K on going from a 100% Ni surface (pure Ni) to the 35% Ni surface. The two desorption peaks labeled A and B are absent on the pure metal spectra and are characteristics of the alloy surfaces. They also shift slightly to a lower temperature with decreasing surface Ni concentration.

In view of the ensemble or local binding site interpretation of the Cu and Ni desorption peaks, peaks A and B are tentatively associated with desorption from mixed Cu–Ni sites. One observation in favor of this association is that of the desorption temperatures. If peaks A and B were truly desorption peaks from mixed Cu–Ni sites, then one would expect them to have activation energies intermediate of the pure metal sites, which was precisely observed. The magnitudes of peaks A and B are comparable to the pure metal peaks, which indicates that the mixed Cu–Ni sites are as numerous as the pure metal sites. Note that the interpretation of the desorption spectrum in terms of the ensemble effect does not presuppose any particular binding site configuration. The one necessary condition for this interpretation to hold is that the surface must be reasonably homogeneous, because only on

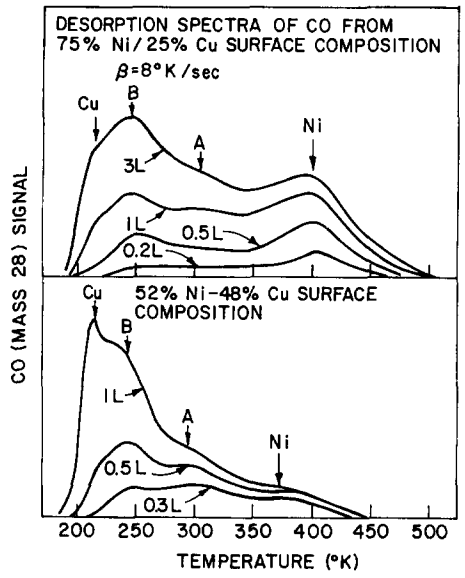

FIG. 3. Thermal desorption spectra of CO from 75% Ni-25% Cu and 52% Ni-48% Cu alloy surfaces as a function of exposures. Three Langmuirs is the saturation exposure (not shown for the 52% Ni-48% Cu surface).

such a surface can the number of mixed Cu–Ni sites be comparable to the pure metal sites.

The observation of peaks A and B, as well as the movement of the Ni desorption peak with surface compositions, furnish strong arguments that large amounts of clustering or islanding is absent on the alloy surfaces. If islanding does occur, one would expect to see only the Cu and Ni desorption peaks. Changing the surface compositions would only change the heights of these peaks, but they would stay at the same temperature.

3. *Ligand Effect on the Strength of the Ni–CO Bond*

The analysis to follow will show that although the major features of the alloy desorption spectra can be explained in terms of the ensemble effect, ligand (long range) effects have to be invoked to account for the striking decrease in the peak temperature of the Ni desorption peak with increasing surface Cu concentration.

To gain some insight into the origin of this decrease in the peak temperature, Fig. 3 shows the desorption spectra on two alloy surfaces at different exposures. The saturation exposure for all the alloy surfaces is approximately 3 L, and this exposure is shown for the 75% Ni–25% Cu surface. Note that for both alloy surfaces, the Ni peak position is essentially independent of exposure (this was true for all compositions studied), which implies first-order desorption with constant activation energy. For first-order desorption, the desorption rate can be written as (*36*, *37*):

$$N(t) = \upsilon C e^{-(\Delta H_a/RT)}$$

where $N(t)$ = desorption rate (molecules/cm^2 sec), υ = frequency factor (sec^{-1}), C = surface coverage (molecules/cm^2), and H_a = activation energy of desorption (kcal/mol). Hence, a peak shift to a lower temperature can be explained by: (1) a significant increase in the frequency factor (a variation in frequency factor of two orders of magnitudes is not uncommon and can result in peak shift as large as 100°K (*37*)), or (2) a decrease in activation energy of desorption. The frequency factor for CO desorption from Ni (110) was accurately measured to be 8.5×10^{15} (*32*). This is quite high compared with the normally assumed 10^{13} frequency factor for a typical first-order desorption. It is unlikely that the frequency factor can be any higher on the alloy surfaces. We conclude that the peak shift is due to a decrease in activation energy. The total peak shift of 80°K on going from 100% Ni surface to 35% Ni surface represents a decrease in 5.5 kcal activation energy. This decrease is correlated with the alloy surface composition alone. The bond between the pure Ni ensemble and the CO molecule, i.e., Ni–CO bond, is weakened by the surrounding Cu atoms.

The Cu–Ni mixed site desorption peaks

also appear to shift downwards in temperature somewhat with increasing surface Cu concentration; however, because of the overlap of the various peaks, it is difficult to obtain quantitative data. In any case, it appears that ligand effects are influencing the mixed binding states. It is more difficult to detect any movement of the Cu desorption peak because the starting temperature of the desorption experiment is not low enough to resolve the entire peak. Hence any shifting of the Cu peak to a lower temperature would not be seen in the present experiment. Intuitively, one would expect the presence of Ni atoms around the Cu–CO bond to strengthen instead of weaken it and to move the desorption peak to a higher temperature. In the present case, such movement should have been apparent in the data but it was not found.

4. Possible CO Desorption Site Configuration on the Alloy Surfaces

On pure Ni, extensive LEED and Auger studies (*33–35, 38*) concerning bonding site configuration have been made. Based on the LEED data, structural models of the CO ad-layer have been proposed. Without extensive LEED beam intensity analysis, the information one can get from LEED patterns are the symmetry and intermolecular distance of the adsorbate overlayer. Henceforth, only reasonable guesses can be made on the geometrical configuration of the binding sites. The many different structural models proposed invariably involve either a bridge site or a fourfold site (*38*). On the (110) surface the three most obvious binding sites are the head-on site, the bridge site, and the fourfold site, with one, two, and four surface atoms in direct contact with the CO molecule, respectively. Due to geometric constraints, a binding site cannot comprise more than four surface atoms. Unless there is significant surface reconstruction accompanying adsorption, or the crystal surface is dominated by steps and kinks (an unlikely event in the present case), the above mentioned sites are the three most probable binding sites. On the alloy surface, a pure Cu or Ni binding site can be either a head-on, a bridge, or a fourfold site, but a mixed Cu–Ni binding site can only be a bridge or a fourfold site.

For the pure metals, it is quite difficult to deduce the binding site configuration from the desorption spectra alone. With the alloys, it is sometimes possible to deduce some information about the binding site coordination, using the surface composition as an extra experimental variable. For the time being, let us assume that only one desorption state is present on the alloy, due to one particular type of binding site. At saturation coverage, the area under the desorption curve gives a measure of the number of such binding sites (assuming binding only occurs at the adsorption sites). By correlating the area under the desorption spectra with surface composition, one can see how the population of this binding site is affected by changing the surface composition. For example, on a random surface with Ni concentration X, the population of adsorption sites consisting of N Ni atoms in proportional to X^N. Hence a log–log plot of saturation coverage versus composition would yield a straight line with slope N. This particular analysis has been shown to work for ethane chemisorption (*39*). Unfortunately, our present CO data is too complicated for analysis of this type. The main problem is that there are too many overlapping adsorption states which means that there is no good way of determining the saturation coverage uniquely. The possible presence of local correlation of the alloy surface atoms (i.e., the tendency of the same kind of atoms to pair up as measured by the short order parameter) (*40*) and adsorbate interaction (*38*) would tend to complicate the analysis as well.

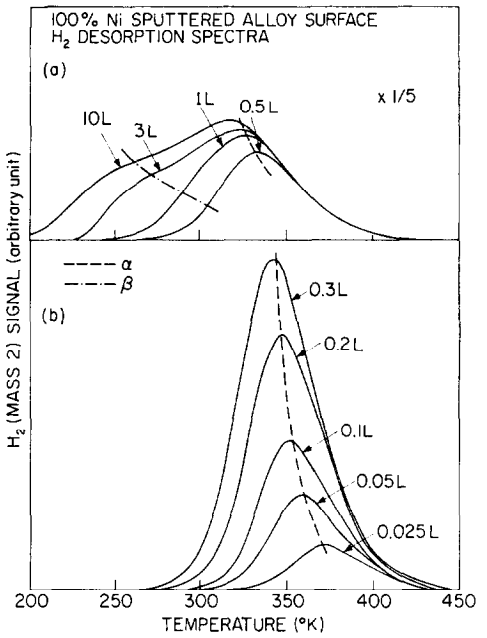

FIG. 4. H_2 desorption spectra of the sputtered 10% Cu–90% Ni bulk composition alloy sample. The surface composition is 100% Ni.

One comment concerning binding site configuration can be made on the CO desorption spectra in Fig. 2. At 35% Ni concentration (Fig. 2g), the Ni desorption peak has not entirely disappeared. This would preclude the fourfold binding site as a viable binding site at low Ni concentration, because the numbers of such sites on the 35% Ni surface are negligibly small. If the binding site configuration does not change with surface Ni concentration, the head-on site or the bridge site are the possible bonding sites on the alloy surface. An examination of the area under the Ni desorption peak for the series of spectra Fig. 2b–g shows that the peak area decreases at a faster rate than a simple linear correlation with surface Ni concentration. Thus, the bridge site appears to be a more likely choice. One can make a similar argument for the pure Cu binding sites. The Cu desorption peak is observable on all surface concentrations, which again suggests that the fourfold site is inappropriate for low Cu concentration surface; the overall concentration dependence of the area under the Cu peaks suggests a "head-on" adsorption site.

E. H_2 DESORPTION FROM Cu–Ni SURFACES

1. Desorption Spectra

The H_2 desorption data are more difficult to interpret than the CO data for two reasons. Comprehensive H_2 desorption data are not available on either pure Ni or Cu. H_2 desorption is second order, and more work is required to extract the activation energy (*36*, *37*). The accuracy to which the activation energy can be determined is also poorer than first-order desorption. For a first-order desorption, a change in activation energy can be readily detected as a direct peak movement, whereas lengthy curve fitting has to be performed for a second-order desorption to extract the same information.

The series of desorption spectra for the sputtered surface of the alloy is shown in Fig. 4. Two adsorption states α and β are resolved. The high temperature desorp-

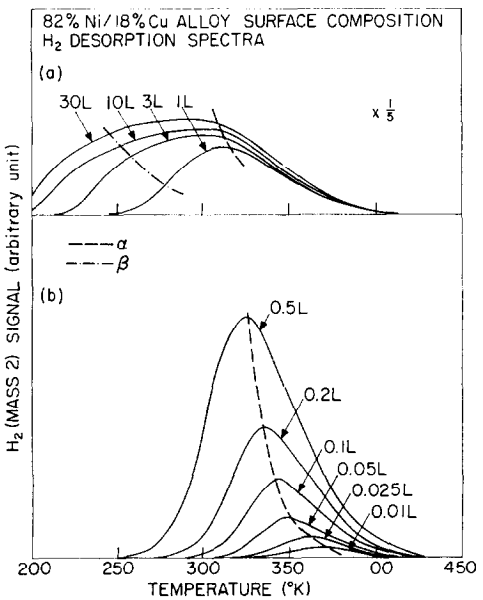

FIG. 5. H_2 desorption spectra of the 82% Ni–18% Cu alloy surface.

tion state α is shown in detail in part (b) of the figure, while both α and β are shown in part (a) (note the reduced vertical scale). The relatively large peak movement with coverage suggests second-order desorption which we will confirm later. At saturation coverage, the H_2 desorption spectrum for the sputtered surface compares favorably with the (110) Ni spectrum (*41*). This is expected because the sputtered surface has a 100% Ni surface composition.

In Figs. 5 and 6, the H_2 desorption spectra on two other alloy surfaces with decreasing surface Ni concentration are presented. (Similar data were also obtained on surfaces of 65% Ni/35% Cu and 52% Ni/48% Cu composition.) Again, the α and β states are observed on all alloy surfaces. As far as one can see, these two states are quite similar to those on the sputtered surface or the pure Ni surface. Such similarity suggests that H_2 adsorption and desorption are controlled by pure Ni binding sites on the alloy surface. Notice too that no desorption states which can be associated with pure Cu or mixed Cu–Ni binding sites are observed.

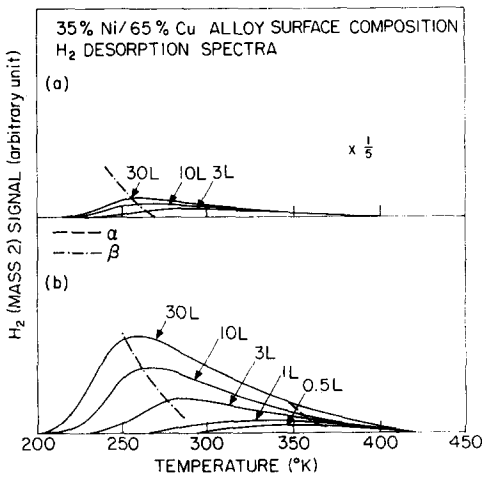

FIG. 6. H_2 desorption spectra of the 35% Ni–65% Cu alloy surface.

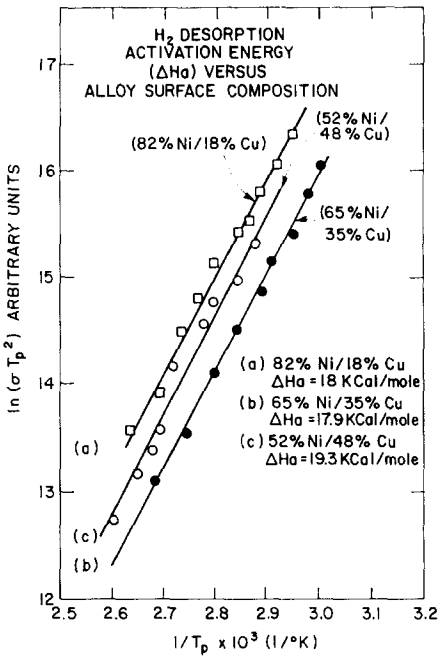

FIG. 7. ln (σT_p^2) versus $1/T_p$ for three alloy surfaces. T_p is the peak temperature in °K for a given coverage (arbitrary unit). The slope of the plot gives the activation energy of desorption.

2. *Activation Energies and Uptake Analyses of the α State*

For a second-order desorption, the activation energy can be determined by plotting ln (σT_p^2) versus $1/T_p$, where T_p is the desorption peak temperature for a given coverage σ. The slope of the straight line obtained gives $\Delta H_a/R$ directly (*36*, *37*), where ΔH_a is the activation energy and R is the Ideal Gas Constant. Such a plot is shown for three alloy surfaces in Fig. 7. The straight lines are linear least square fits for the data points. All the data points shown are for coverages less than 0.3 L; i.e., for each surface, approximately 10 desorption spectra were taken at coverage below 0.3 L. The reason for using coverage less than 0.3 L is that at higher coverage, the β state begins to fill and overlaps the α state, making the determination of the α state peak area and peak temperature all but impossible. Notice that finding the

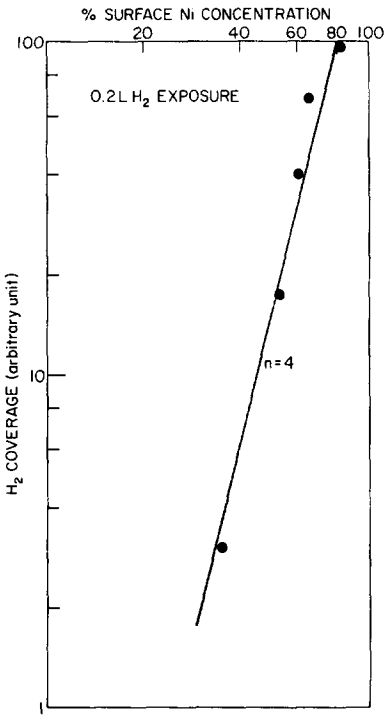

FIG. 8. Log-log plot of the α state H_2 uptake (measured by the area under the desorption curve) versus surface Ni concentration.

activation energy of the α state is possible because the β state is not filled simultaneously with the α state. For the three alloy surfaces, the activation energy of the α state is determined to be 18.5 ± 0.7 kcal/mol. The spread of only ± 0.7 kcal/mol suggests that, to a first approximation, the α state activation energy is not sensitive to surface composition. Since these three alloy surfaces only span a Ni concentration of $\simeq$30%, more experiments have to be performed on a wider range of alloy surface compositions to validate the conclusion.

The uptake of H_2 in the α state decreases drastically with decreasing surface Ni concentration. This is illustrated in Fig. 8, where the H_2 uptake (area under the thermal desorption curve) for a 0.2 L exposure of H_2 is plotted versus surface Ni concentration in a log–log scale. Uptake is found to be proportional to the fourth power of surface Ni concentration. This is also found to be true for lower exposures. At higher exposures, the β state begins to fill and makes this analysis impossible.

The dissociation of the H_2 molecule on adsorption on the alloy surfaces is necessary to give rise to the second-order desorption observed. It is known that H_2 does not adsorb on Cu, even at low temperatures. This has been attributed to the failure of the Cu surface atoms to dissociate the H_2 molecule. Therefore, the striking fourth power versus composition dependence can be explained by assuming that the dissociation of a H_2 molecule on the alloy surface requires a fourfold site. Thus, even though the hydrogen atom may eventually bind on the alloy surface on a differently coordinated site (e.g., head-on or bridge), it is the dissociation on a four-folded site which determines the uptake of the state.

3. *Uptake of the β State*

Similar to the α state, the β state peak position also moves with coverage. At high coverages, the β state is not fully resolved. Since the β state begins to fill only after the α state is filled, no activation energy analysis can be performed on it. The uptake of H_2 in the β state decreases as the surface Ni concentration decreases, but it does so at a slower rate than the α state. For the high Ni concentration surfaces (Figs. 4 and 5) the area under the α state at saturation ($\simeq$10 L) is higher than the β state. For the 65% Ni–35% Cu surface, the area under tha α state is approximately the same as that under the β state. For the low Ni concentration surface (Fig. 6), the area under the α state is definitely less than that under the β state.

Since the α state is filled approximately above 300°K and the β state below that, the α state would not be filled at all if the experiment is carried out at room temperature. The behavior of the α and β state approximately corresponds to the

strongly chemisorbed and weakly chemisorbed state reported in the literature (*2*). In particular, if a low pressure ($\simeq 10^{-6}$ Torr) titration experiment is performed on the alloy surface at room temperature, the measured uptake would be that of the α state only and one might get a similar fourth power dependence with surface composition. However, further experimentation is necessary to clarify this aspect of the hydrogen titration on single crystal Cu–Ni alloy.

F. CONCLUSION

To summarize, the bonding of CO and H_2 on the Cu–Ni alloy has been studied by thermal desorption spectroscopy, augmented by Auger spectroscopy. A novel method to prepare alloy surfaces of different compositions from the same bulk sample was developed. First, the sample was sputtered with an argon ion beam to deplete the surface Cu concentration. Then, it was annealed in a temperature range (440 to 650°C) where the surface composition was controlled by bulk diffusion (i.e., diffusion of Cu atoms from the bulk of the sample to the surface). The desorption order and energies for CO and H_2 were determined on these alloy surfaces and the major findings are listed below.

(a) CO desorption is first order and four desorption states are identified. The highest and lowest activation energy states are attributed to desorption from pure Ni and pure Cu ensembles (binding sites). Two intermediate activation states are attributed to desorption from mixed Cu–Ni ensembles (binding sites).

(b) The activation energy of the pure Ni binding sites decreases linearly with increasing surface Cu concentration, indicating that non-nearest neighbor Cu atoms weaken the Ni–CO bond. This ligand effect (long range effect) accounts for a 20% decrease in the Ni–CO energy on going from a 100% Ni surface to a 35% Ni surface.

(c) H_2 desorption is second order. Two desorption states which are similar to those observed on pure Ni are found. For a given exposure of H_2, the uptake of the high temperature state decreases in proportion to the fourth power of surface Ni concentration.

(d) The activation energy of the high temperature H_2 binding state (18.5 ± 0.7 kcal/mol) is constant with alloy surface composition.

The findings show that both the ensemble effect and the ligand effect are present in the bonding of CO on the alloy. By and large, the ensemble effect is the dominant effect and the ligand effect only affects the bond strength in second order. Likewise, the H_2 desorption data show that it is necessary to invoke the ensemble effect to explain the data. However, the fact that there is no measurable variation in the activation energies with surface compositions implies that the ligand effect may be very weak or absent.

ACKNOWLEDGMENTS

Valuable discussions with Prof. M. Boudart and Prof. R. Madix are gratefully acknowledged.

This work was supported by the National Science Foundation Grant No. DMR 74-22230. One of the authors (DTL) gratefully acknowledges a fellowship from the Fannie and John Hertz Foundation.

REFERENCES

1. Sinfelt, J. H., *J. Catal.* **29**, 308 (1973).
2. Sinfelt, J. H., Carter, J. L., and Yates, D. J. C., *J. Catal.* **24**, 283 (1972).
3. Baker, M. McC., and Jenkins, G. I., *Adv. Catal.* **7**, 1 (1955).
4. Hall, W. K., and Emmett, P. H., *J. Phys. Chem.* **62**, 816 (1958).
5. Van Der Plank, P., and Sachtler, W. M. H., *J. Catal.* **7**, 300 (1967).
6. Campbell, J. S., and Emmett, P. H., *J. Catal.* **7**, 252 (1967).
7. Degras, P. A., *in* "Molecular Process on Solid Surfaces" (E. Drauglis, R. D. Gretz, and R. I. Jaffee, Eds.). McGraw-Hill, New York, 1969.
8. Van Santen, R. A., *Surf. Sci.* **53**, 35 (1975).

9. Sachtler, W. M. H., *Vide* **164**, 67 (1973).
10. Kuen, E., *J. Vac. Sci. Tech.* **8**, 57 (1971).
11. Paulsen, R. H., and Schreiffer, J. R., *Surf. Sci.* **48**, 329 (1975).
12. Sachtler, W. M. H., *J. Vac. Sci. Tech.* **9**, 828 (1971).
13. Sachtler, W. M. H., Dorgelo, G. J. H., and Jongepier, R., *J. Catal.* **4**, 100 (1965).
14. Sachtler, W. M. H., and Dorgelo, G. H. H., *J. Catal.* **4**, 654 (1965).
15. Sachtler, W. M. H., and Jongepier, R., *J. Catal.* **4**, 665 (1965).
16. Van Der Plank, P., and Sachtler, W. M. H., *J. Catal.* **12**, 35 (1968).
17. Soma-Noto, Y. and Sachtler, W. M. H., *J. Catal.* **34**, 162 (1974).
18. Takasu, T., and Yamashima, J., *J. Catal.* **28**, 171 (1973).
19. Sachtler, W. M. H., and Van Der Plank, P., *Surf. Sci.* **18**, 62 (1969), and references therein.
20. Seib, D. H., and Spicer, W. E., *Phys. Rev.* **B2**, 1676 (1970); *Phys. Rev.* **B2**, 1694 (1970).
21. Stock, G. M., Williams, R. W., and Faulkner, J. S., *Phys. Rev.* **B4**, 4390 (1971), and references therein.
22. Bassil, A., Ehrenreich, H., Schwartz, L., and Watson, R. E., *Phys. Rev.* **B9**, 445 (1974).
23. Helms, C. R., *J. Catal.* **35**, 114 (1975).
24. Helms, C. R., and Yu, K. Y., *J. Vac. Sci. Tech.* **12**, 276 (1975).
25. Helms, C. R., Yu, K. Y., and Spicer, W. E., *Surf. Sci.* **52**, 217 (1975).
26. Van Santen, R. A., and Boersma, M. A. M., *J. Catal.* **34**, 13 (1974).
27. (a) Williams, F. L., and Boudart, M., *J. Catal.* **30**, 438 (1973); (b) Williams, F. L., and Nason, P., *Surf. Sci.* **45**, 377 (1974).
28. Burton, J. J., Hyman, E. A., and Fedak, D. G., **37**, 106 (1975).
29. Moss, S. C., *Phys. Rev. Lett.* **23**, 38 (1969).
30. Buytymowicz, D. R., Manning, J. R., and Read, M. E., *J. Phys. Chem. Ref. Data* **2**, 643 (1973).
31. Tarng, M. L., and Wehner, G. K., *J. Appl. Phys.* **42**, 2449 (1971).
32. Falconer, J., and Madix, R. J., *Surf. Sci.* **48**, 393 (1975).
33. Tracy, J. C., *J. Chem. Phys.* **56**, 2748 (1972).
34. Tracy, J. C., *J. Chem. Phys.* **56**, 2736 (1972).
35. Christmann, K., Schober, O., and Ertl, G., *J. Chem. Phys.* **60**, 4719 (1974).
36. Redhead, P. A., *Vacuum* **12**, 203 (1962).
37. Ehrlich, G., *Adv. Catal.* **14**, 255 (1963).
38. Ertl, E., and Kuppers, J., "Low Energy Electrons and Surface Chemistry," pp. 224–230. Verlag Chemie, Weinheim GmbH, D-694, 1974.
39. Burton, J. J., and Hyman, E., *J. Catal.*, to be published.
40. Nix, F. C., and Shockley, W., *Rev. Mod. Phys.* **10**, 1 (1938).
41. Falconer, J., Unpublished Ph.D. Thesis, Stanford University, 1974, p. 38.
42. Cardillo, M. J., Balooch, M., and Stickney, R. E., *Surf. Sci.* **50**, 263 (1975).